Extension of the 'solid-shell' concept for application to large elastic and large elastoplastic deformations

R. Hauptmann, K. Schweizerhof[*,†] and S. Doll

Institute of Mechanics, University of Karlsruhe, Kaiserstr. 12, 76128 Karlsruhe, Germany

SUMMARY

In the present contribution we extend a previously proposed so-called solid–shell concept which incorporates only displacement degrees of freedom to the simulation of large elastic and large elastoplastic deformations of shells. Therefore, the modifications necessary for hyper-elastic or elastoplastic material laws are discussed. These modifications concern the right Cauchy–Green tensor for large elastic deformations, respectively, the deformation gradient for elastoplasticity which then are consistent to the modified Green–Lagrange strains that are necessary for transverse shear and membrane locking free solid–shell element formulations.

However, in addition to the locking mentioned above especially in the range of plasticity incompressibility locking becomes important. Thus, the second major aspect of this contribution is the discussion of several ways to avoid incompressibility locking also including the investigation of eigenmodes. Finally, a selective reduced integration scheme with reduced integration for the volumetric term is employed and described in detail, although it is limited to material laws which allow the decomposition into a volumetric and a deviatoric part. Some numerical examples show the range of application for the proposed elements. Copyright © 2000 John Wiley & Sons, Ltd.

KEY WORDS: non-linear finite element analysis; shell element technology; plasticity; hyper-elasticity; incompressibility locking

1. INTRODUCTION

General shell structures contain flat, slightly and highly curved parts. They also consist of parts with dominantly two- or general three-dimensional (2D or 3D) stress states. The analyses of their linear and non-linear behaviour should be accurate and efficient. It is therefore desirable to combine different element types, such that the calculation of each part is as efficient and as accurate as possible.

Most efficient shell elements are based on the degenerated shell concept (see e.g. References [1–3]). The starting point of this shell concept is the kinematics of the three-dimensional continuum modified by the three following assumptions and resulting in a mid-surface description

---

[*]Correspondence to: K. Schweizerhof, Institut fur Mechanik, Universitat Karlsruhe (TH), Kaiserstr. 12, 76128 Karlsruhe, Germany
[†]E-mail: karl.schweizerhof@bau-verm.uni-karlsruhe.de

in analogy to standard shell theory (see References [4, 5]). First, the normals to the mid-surface in the initial configuration remain straight but not normal during the deformation. Second, the thickness of the element remains constant and third the normal stress in thickness direction is neglected. Although these approximations lead to very good results in most cases, there could arise difficulties concerning the rotational degrees of freedom. In particular, when describing the boundary conditions, special care of the nodal co-ordinate systems must be taken and a complicated update of the rotations is necessary in geometrically non-linear situations. Additional problems arise when shell elements are used in combination with solid elements. However, the most important difficulty occurs in using general three-dimensional material laws due to the requirement to reduce the material law according to the normal stress condition.

The solid–shell concept presented previously in detail in Reference [6] and proposed by Büchter et al. [7], Parisch [8], Seifert [9], Verhoeven [10] in a slightly different form that has proven to avoid the disadvantages mentioned above and the linear and geometrically non-linear analyses in Reference [6] and further studies have shown no misbehaviour so far for small strain problems. Therefore, in the present contribution the application of the solid–shell concept to large elastic and large elastoplastic deformations is described.

First the solid–shell concept is applied to compressible large elastic deformations. Therefore, the most general, originally incompressibility Ogden material law [11, 12] with compressible extension is introduced. This material law includes also the Neo-Hooke [13] and Mooney–Rivlin [14] elastic material laws as special cases.

Then large elastoplastic deformations are considered. Therefore, the commonly used Hencky material law with isotropic von Mises plasticity [15] is employed to the solid–shell formulations. However, as known from solid elements the problem of incompressibility locking arises.

So far, there are three promising approaches known to avoid this incompressibility locking.

The first one proposed originally by Moran et al. [16] is based on a modification of the deformation gradient. However, this modification leads to rather complicated expressions, when a consistent linearization is performed, and therefore it cannot be applied easily to existing element formulations.

The second one, well known as reduced integration and also removing transverse shear and membrane locking (see e.g. Reference [10]) leads to element formulations that exhibit additional undesired zero-energy modes. To overcome this defect special stabilization techniques (see e.g. Reference [17]) can be applied. However, the resulting elements are based mostly on penalty parameters and therefore are not very reliable. Solely, the element based on a quadratic Serendipity displacement interpolation in in-plane direction contains only two zero energy modes that cannot appear in most FE meshes and is somehow more reliable.

In the current contribution, the selective reduced integration of the volumetric term is chosen which is described in Reference [18] for the finite elastic case and in Reference [19] for 3D-continuum problems in the case of finite elastoplasticity including viscoplasticity. Then, as obtained in References [18, 19] for the solid elements no undesired zero-energy modes are found and locking free solid–shell element formulations result. Essential for this approach is that the material laws used must allow a split into volumetric and deviatoric parts. However, the commonly employed material laws can be easily split and thus this limitation is no real disadvantage at the moment.

The concluding numerical examples are chosen to demonstrate the capabilities of the solid–shell concept in the range of large elastic and large elastoplastic deformations. There is also a focus on the eigenmodes and eigenvalues of single elements to gain more insight in particular in the case of incompressibility.

2. A SHORT REVIEW OF THE SOLID–SHELL CONCEPT

In this section, the main features of a shell concept which employs only displacement degrees of freedom and thus allows to overcome the known problems associated with the rotational degrees of freedom and the plane stress assumption both incorporated by degenerated shell elements are outlined. For a more detailed description see Reference [6]. Solely the assumption of the degenerated shell concept that the normals to the element mid-surface remain straight but not necessarily normal during the deformation is adopted by the solid–shell concept. Thus, the initial 3D continuum of the shell geometry

$$\mathbf{X}(\xi,\eta,\zeta) = \tfrac{1}{2}\{(1+\zeta)\mathbf{X}_{\mathrm{u}}(\xi,\eta) + (1-\zeta)\mathbf{X}_{\mathrm{l}}(\xi,\eta)\} \tag{1}$$

and the displacements

$$\mathbf{u}(\xi,\eta,\zeta) = \mathbf{T}^{-1}(\xi,\eta)\mathbf{\Theta}(\zeta)\begin{bmatrix} \mathbf{T}(\xi,\eta) & \mathbf{0}_{3\times3} & \mathbf{0}_{3\times n} \\ \mathbf{0}_{3\times3} & \mathbf{T}(\xi,\eta) & \mathbf{0}_{3\times n} \\ \mathbf{0}_{n\times3} & \mathbf{0}_{n\times3} & \mathbf{1}_{n\times n} \end{bmatrix}\begin{pmatrix} \mathbf{u}_{\mathrm{u}}(\xi,\eta) \\ \mathbf{u}_{\mathrm{l}}(\xi,\eta) \\ \boldsymbol{\beta}(\xi,\eta) \end{pmatrix} \tag{2}$$

are approximated in global Cartesian co-ordinates $(\mathbf{e}_1,\mathbf{e}_2,\mathbf{e}_3)$. In Equations (1) and (2) the approximation in in-plane direction is decoupled from the approximation in thickness direction. Due to the transformation matrix $\mathbf{T}$ from global to local co-ordinates aligned to the shell geometry the approximation in thickness direction of the local displacements in in-plane direction can be chosen independently from the approximation of the local displacement in thickness direction. An obvious possibility to fulfill the assumption cited above, can be achieved by the following matrix $\mathbf{\Theta}(\zeta)$, which contains the linear interpolation of all three local displacements in thickness direction:

$$\mathbf{\Theta}(\zeta) = \frac{1}{2}\begin{bmatrix} 1+\zeta & 0 & 0 & 1-\zeta & 0 & 0 \\ 0 & 1+\zeta & 0 & 0 & 1-\zeta & 0 \\ 0 & 0 & 1+\zeta & 0 & 0 & 1-\zeta \end{bmatrix} \tag{3}$$

It must be noted that with this interpolation the transformation matrix $\mathbf{T}$ can be omitted leading to a displacement approximation equal to the geometry approximation (1). According to the degenerated shell concept ξ and η are local convective co-ordinates in in-plane direction and ζ is the local convective co-ordinate in thickness direction. The position $\mathbf{X}$ and the displacements $\mathbf{u}$ of each point of the shell is described by a position vector $\mathbf{X}_{\mathrm{u}}$ and displacements $\mathbf{u}_{\mathrm{u}}$ of the corresponding points on the upper shell surface and on the lower shell surface $\mathbf{X}_{\mathrm{l}}$ and $\mathbf{u}_{\mathrm{l}}$. For the approximation of displacements (2) additional degrees of freedom belonging to a hierarchical interpolation are employed. However, using the interpolation in thickness direction described in Equation (3) no additional degrees of freedom $\beta(\xi,\eta)$ are required. Applying the
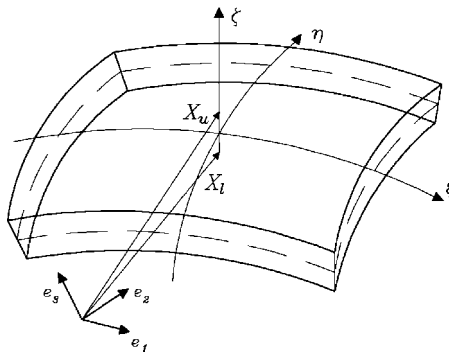
Figure 1. Geometry of the solid–shell element.

relation $\mathbf{x} = \mathbf{X} + \mathbf{u}$, the geometry in the actual state which is essential for the evaluation of the deformation gradient

$$\mathbf{F} = \frac{\partial \mathbf{x}}{\partial \mathbf{X}} \tag{4}$$

can be computed.

Contrary to the kinematics used for degenerated shell elements the weak form

$$\delta \Pi = \int_V \delta \mathbf{E} \cdot \mathbf{S} \, dV + \delta \Pi_{\text{ext}} = 0, \quad \delta \Pi_{\text{ext}} \ \ldots \ \text{external work} \tag{5}$$

contains the complete Green–Lagrange strain tensor $\mathbf{E}$ and the corresponding second Piola–Kirchhoff stress tensor $\mathbf{S}$. Thus, it is possible to compute the thickness change due to forces in thickness direction and to apply general 3D material laws without any modification.

2.1. Efficient locking free, materially linear solid–shell element formulations

Degenerated shell elements or solid–shell elements can be considered to be completely locking free, if the order of approximation for all displacements is fairly high at least of the order of 4 or 5 [20]. Orders up to 8 provide even better convergence [20], though this is problem dependent and clearly also a function of mesh density. However, elements based on such high-order shape functions are difficult to handle, less robust in the non-linear range and rather inefficient. Therefore, various methods to avoid locking by enhancing a linear, quadratic or cubic displacement approximation have been developed in the past [8, 21–23].

2.1.1. Transverse shear and membrane locking. In our contribution, the method of assumed strains is applied to solid–shell element formulations with a bilinear approximation in in-plane direction. Thus, the following interpolation as proposed by Bathe and Dvorkin [24] to reduce the transverse shear locking is used:

$$E_{\xi\zeta}^{\text{as}} = \tfrac{1}{2}(1 - \eta)E_{\xi\zeta}^A + \tfrac{1}{2}(1 + \eta)E_{\xi\zeta}^C \quad E_{\eta\zeta}^{\text{as}} = \tfrac{1}{2}(1 - \xi)E_{\eta\zeta}^D + \tfrac{1}{2}(1 + \xi)E_{\eta\zeta}^B \tag{6}$$

The essential assumption of the assumed natural strain concept is to assume the transverse shear interpolation in local convective co-ordinates to be constant in ξ and linear in the η direction for $E_{\xi\zeta}^{\text{as}}$, respectively, to be constant in η and linear in the ξ direction for $E_{\eta\zeta}^{\text{as}}$.

A slightly superior performance of this element formulation can be achieved by additional enhancements of the in-plane strains according to the enhanced assumed strain (EAS) method [25]. Therefore, the functions suggested by Taylor and Wilson [26] and Braun [27] are adopted:

$$
\mathbf{E}_{ip} = \begin{pmatrix} E_{\xi\xi} \\ E_{\eta\eta} \\ 2E_{\xi\eta} \end{pmatrix} = \mathbf{E}_{ip}^k + \tilde{\mathbf{E}}_{ip} = \mathbf{E}_{ip}^k + \mathbf{M}\alpha
$$

$$
= \begin{pmatrix} E_{\xi\xi} \\ E_{\eta\eta} \\ 2E_{\xi\eta} \end{pmatrix}_k + \frac{1}{\det \mathbf{J}} \begin{bmatrix} t_{11}^2 & t_{12}^2 & t_{11}t_{12} \\ t_{21}^2 & t_{22}^2 & t_{21}t_{22} \\ 2t_{11}t_{21} & 2t_{12}t_{22} & t_{11}t_{22}+t_{12}t_{21} \end{bmatrix} \begin{bmatrix} \xi & 0 & 0 & 0 \\ 0 & \eta & 0 & 0 \\ 0 & 0 & \xi & \eta \end{bmatrix} \begin{pmatrix} \alpha_1 \\ \alpha_2 \\ \alpha_3 \\ \alpha_4 \end{pmatrix} \quad (7)
$$

In Equation (7) the vector $\mathbf{E}_{ip}^k$ contains the in-plane Green–Lagrange strains, $\det \mathbf{J}$ is the determinant of the Jacobian of the transformation in isoparametric space and the vector α consists of independent parameters that are condensed out on element level. The factors

$$
t_{\alpha\beta} = \mathbf{G}_\alpha(\xi,\eta,\zeta) \cdot \mathbf{G}^\beta(0,0,0), \quad \alpha,\beta = 1,2 \quad (8)
$$

are used to transform the enhanced strains to the covariant co-ordinate system at the element mid-point which is necessary to obtain unique values for the parameters α_i. The vectors $\mathbf{G}_i$ and $\mathbf{G}^i$ in Equation (8) are the base vectors of the covariant, respectively, contravariant co-ordinate system.

For 9- or 16-node degenerated shell elements the assumed strain approximation proposed by Bucalem and Bathe [21] leads to remarkably good results [28] so that this approximation is recommended for solid–shell element formulations using a biquadratic or bicubic Lagrange displacement approximation in tangent space, see e.g. Reference [28]. As is well known, solely for the element formulation with a quadratic Serendipity displacement approximation in the ξ and η directions the reduced integration scheme in tangent space leads to a membrane and transverse shear locking free element [10] but contains two zero-energy modes. However, both kinematical modes do not occur in most meshes and therefore the corresponding 16 node solid–shell element works quite well in most cases.

2.1.2. Thickness locking. According to investigations in the literature (see e.g. References [29, 27]), a formulation with a linear w' displacement assumption in thickness direction tends to so-called thickness locking, which also will be observed in the numerical analyses. This undesired locking occurs due to the constant approximation of the strain $E_{\zeta\zeta}$ in thickness direction contrary to a linear $S^{\zeta\zeta}$ stress distribution found when bending occurs. The reason for the $E_{\zeta\zeta}$ varying linearly in thickness direction is the coupling between the linear in-plane strains and the normal stress in thickness direction, if the Poisson ratio is not equal to zero (see Figure 2).

One way to overcome this limitation is to apply the condition $S^{\zeta\zeta} = 0$ for the normal stresses according to the degenerated shell concept. Thus, the term $\delta E_{\zeta\zeta}S^{\zeta\zeta} = 0$ originally included in the weak form (5) vanishes and a zero-energy mode in thickness direction results. By adding a stiffness in thickness direction with neglecting the coupling between the normal in-plane strains and the normal thickness strain the undesired zero-energy mode can be avoided. In

$$S^{\zeta\zeta} = \lambda E_{\xi\xi} + (\lambda + 2\mu)E_{\zeta\zeta}$$

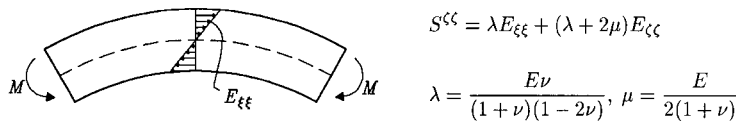$$\lambda = \frac{E\nu}{(1+\nu)(1-2\nu)}, \quad \mu = \frac{E}{2(1+\nu)}$$

Figure 2. Beam subjected to bending moments.

the case of the linear elastic St-Venant–Kirchhoff material law this is achieved by simply inserting the Poisson ratio $\nu = 0.0$ into

$$S^{\zeta\zeta} = \lambda E_{\xi\xi} + \lambda E_{\eta\eta} + (\lambda + \mu)E_{\zeta\zeta} \tag{9}$$

finally leading to the modified weak form

$$\int_V \delta \mathbf{E} \cdot \mathbf{S}\, \mathrm{d}V + \int_V \delta E_{\zeta\zeta}\mu(\nu=0.0)E_{\zeta\zeta}\, \mathrm{d}V = 0 \tag{10}$$

For simplicity, it is assumed in Equations (9) and (10) and Figure 2 that the convective co-ordinate system is a Cartesian such that $\mathbf{G}_i \cdot \mathbf{G}_j = \mathbf{G}^i \cdot \mathbf{G}^j = 0$ vanishes for $i \neq j$.

Concerning plasticity for small deformations the first term in Equation (10) can be evaluated as for degenerated shell elements and the second term can be handled as for one-dimensional (1D) plasticity which is used, e.g. for truss elements. However, rather complicated modifications must be applied to general 3D material laws and therefore this approach is limited to linear elasticity or plasticity for small deformations and not described here in detail.

Instead, the assumption of a linear distribution of the normal strain in thickness direction over the thickness is proposed. This could be achieved by a modification of the matrix containing the interpolation in thickness direction (3):

$$\bar{\mathbf{\Theta}}(\zeta) = \frac{1}{2}\begin{bmatrix} 1+\zeta & 0 & 0 & 1-\zeta & 0 & 0 & 0 \\ 0 & 1+\zeta & 0 & 0 & 1-\zeta & 0 & 0 \\ 0 & 0 & 1+\zeta & 0 & 0 & 1-\zeta & \boxed{1-\zeta^2} \end{bmatrix} \tag{11}$$

such that a quadratic approximation of the displacement in thickness direction results as suggested in Reference [30] and in as slightly different form in References [29, 9]:

$$\mathbf{u}(\xi,\eta,\zeta) = \mathbf{T}^{-1}(\xi,\eta)\bar{\mathbf{\Theta}}(\zeta)\begin{bmatrix} \mathbf{T}(\xi,\eta) & \mathbf{0}_{3\times3} & \mathbf{0}_{3\times1} \\ \mathbf{0}_{3\times3} & \mathbf{T}(\xi,\eta) & \mathbf{0}_{3\times1} \\ \mathbf{0}_{1\times3} & \mathbf{0}_{1\times3} & 1 \end{bmatrix}\begin{pmatrix} \mathbf{u}_\mathrm{u}(\xi,\eta) \\ \mathbf{u}_\mathrm{l}(\xi,\eta) \\ \beta(\xi,\eta) \end{pmatrix} \tag{12}$$

Thus, this solid–shell element formulation shows an additional degree of freedom per edge (see Figure 3).

Another approach is to enhance the constant normal strain in thickness direction by a linear extension over the thickness according to the EAS method, as proposed in References [7, 27]:

$$E_{33} = E_{33}^k + \hat{\mathbf{M}}\hat{\boldsymbol{\alpha}} = E_{33}^k + \zeta\frac{1}{\det \mathbf{J}}\begin{bmatrix} 1 & \xi & \eta & \xi\eta \end{bmatrix}\begin{pmatrix} \hat{\alpha}_1 \\ \hat{\alpha}_2 \\ \hat{\alpha}_3 \\ \hat{\alpha}_4 \end{pmatrix} \tag{13}$$
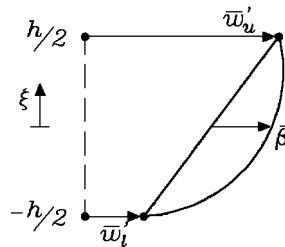
Figure 3. Hierarchical quadratic interpolation in the ζ direction.

A similar formulation was suggested by Parisch [8]. For solid–shell element formulations with a linear displacement approximation in in-plane direction the transformation to a co-ordinate system in the centre of the element can be omitted. However, if higher-order elements in tangent space are concerned a co-ordinate system varying over the element area must be taken into account by adding the factor t_{33}^2 to the matrix $\hat{\mathbf{M}}$ (13) in analogy to Equations (7) and (8).

2.1.3. Curvature Locking. If the directions of the vectors from the lower to the upper nodes at the edges are not perpendicular to the midsurface of the element, the so-called curvature locking appears in bending situations. This is particularly obvious for thin solid–shells. A perfect remedy is a bilinear interpolation of the thickness strains $E_{\zeta\zeta}$ in in-plane direction as proposed by Betsch and Stein [36] and is therefore also implemented in the solid–shell elements. In the numerical examples discussed in Chapter 5 this locking effect is of minor importance and thus not further investigated in the current contribution.

3. CONSIDERATIONS CONCERNING LARGE ELASTIC DEFORMATIONS

Contrary to the St-Venant–Kirchhoff material law which is only valid for small elastic deformations large elastic deformations can be computed using, e.g. the Neo-Hooke [13], Mooney–Rivlin [14] or Ogden [11] material law. The most general of these three material laws is the Ogden material law which includes the two other material laws as special cases. Although the Ogden material law is introduced only briefly its application to the various locking free solid–shell formulations is described in detail here. For an extensive discussion of hyperelastic materials and large deformations, it is referred in Reference [31].

3.1. Ogden material law with compressible extension

For elastic deformations the stresses $\mathbf{S}$ are computed by partial differentiation of a strain energy density function W to the Green–Lagrange strains $\mathbf{E}$:

$$\mathbf{S} = \frac{\partial W}{\partial \mathbf{E}} \tag{14}$$

In this contribution for the originally incompressible Ogden material law [23] a compressible extension also proposed by Ogden [12] is employed. Thus, the incorporated strain energy

density function W can be split additively into the original Ogden strain energy density function W_{OG} and the compressible extension W_{comp},

$$W = W_{OG} + W_{comp} \tag{15}$$

The Ogden material model is based on the incompressible strain energy density function

$$W_{OG} = \sum_{i=1}^{3} \frac{\mu_i}{\alpha_i} \left(\lambda_1^{\alpha_i} + \lambda_2^{\alpha_i} + \lambda_3^{\alpha_i} - 3 \right) \tag{16}$$

with the principal stretches λ_i and the parameters μ_i and α_j which have to be determined by material testing. However, it must be noted that for small deformations the St-Venant–Kirchhoff material law must be included. Thus, the condition

$$\sum_{i=1}^{3} \alpha_i \mu_i = 2\mu \tag{17}$$

limits the choice of the parameters α_i and μ_i. In Equation (17), μ is the Lamé constant, respectively, the shear modulus $G = \mu$. If the parameters are chosen such that $\mu_1 = \mu$, $\alpha_1 = 2$ and $\mu_2 = \mu_3 = 0$ the Neo-Hooke material law is obtained.

Following Equation (15), the compressible strain energy density function

$$W_{comp} = -\sum_{i=1}^{3} \mu_i \ln J + \Lambda \beta^{-2} \left(\beta \ln J + J^{-\beta} - 1 \right), \quad J = \lambda_1 \lambda_2 \lambda_3 \tag{18}$$

is added to the Ogden energy function (16). Here the ratio of compressibility can be chosen by the additional parameter Λ.

3.2. Right Cauchy–Green tensor consistent to the modified strains

The principal stretches which are needed in Equations (16) and (18) are computed by a spectral decomposition of the right Cauchy–Green tensor

$$\mathbf{C} = \sum_{j=1}^{3} \lambda_j^2 \, \mathbf{N}_j \otimes \mathbf{N}_j \; \Rightarrow \; \lambda_j \tag{19}$$

Considering the element kinematics as a function of the total displacements the right Cauchy–Green tensor

$$\mathbf{C} = \mathbf{F}^T \mathbf{F} \tag{20}$$

is computed using the deformation gradient $\mathbf{F}$ introduced in Equation (4).

However, special considerations are required for the computation of the right Cauchy–Green tensor, if techniques are applied that lead to the locking free solid-shell formulations described in Section 2.1. Thus, these formulations can be written such that they are based on strains $\mathbf{E}^{mod}$ which are the result of a modification of the Green–Lagrange strains $\mathbf{E}$. In equivalence to total displacement formulations the relationship between the modified Green–Lagrange strains $\mathbf{E}^{mod}$ and the corresponding right Cauchy–Green tensor $\mathbf{C}^{mod}$ shows the form

$$\mathbf{E}^{mod} = \tfrac{1}{2}(\mathbf{C}^{mod} - \mathbf{1}) \tag{21}$$

which immediately leads to

$$\mathbf{C}^{mod} = 2\mathbf{E}^{mod} + \mathbf{1} \tag{22}$$

Finally, the modified right Cauchy–Green tensor

$$\mathbf{C}^{\mathrm{mod}} = \sum_{j=1}^{3} \lambda_j^2 \, \mathbf{N}_j \otimes \mathbf{N}_j \; \Rightarrow \; \lambda_j \tag{23}$$

is employed to compute the principal stretches λ_j by spectral decomposition. The latter are required for the evaluation of the strain energy density functions (16) and (18).

4. CONSIDERATIONS CONCERNING LARGE ELASTOPLASTIC DEFORMATIONS

In this contribution the classical Hencky material law [32] with isotropic von Mises plasticity [15] for large elastoplastic deformations is employed to various solid-shell element formulations. Essential for this material algorithm are the rate independency and the multiplicative decomposition of the deformation gradient

$$\mathbf{F} = \mathbf{F}^{\mathrm{el}} \mathbf{F}^{\mathrm{pl}} \tag{24}$$

In equivalence to the previously introduced solid-shell element formulations the weak form (5) is evaluated in the reference configuration and thus the deformation gradient $\mathbf{F}$ is also necessary for the push forward and pull backward operations. A detailed description of this material law together with special algorithmic aspects is given in Reference [19].

4.1. Deformation gradient consistent to modified strains

As already discussed in Section 3.2 locking free solid-shell element formulations are based on modified strains $\mathbf{E}^{\mathrm{mod}}$ (see Equation (21)). Therefore, a modified deformation gradient $\mathbf{F}^{\mathrm{mod}}$ which is consistent to the modified strains $\mathbf{E}^{\mathrm{mod}}$ is inserted into the material algorithm for large elastoplastic strains. Thus, the big advantage of this approach is that all algorithms concerning the material can be adopted from solid elements without any modification. However, the evaluation of the modified deformation gradient $\mathbf{F}^{\mathrm{mod}}$ is rather time-consuming which is outlined in the following.

If the deformation gradient

$$\mathbf{F} = \mathbf{R}\mathbf{U} \tag{25}$$

which can be split into a right-stretch tensor $\mathbf{U}$ and an orthogonal rotation tensor $\mathbf{R}$ is inserted into the Green–Lagrange strains

$$\mathbf{E} = \tfrac{1}{2}\big(\mathbf{F}^{\mathrm{T}}\mathbf{F} - \mathbf{1}\big) \tag{26}$$

the orthogonal rotation tensor $\mathbf{R}$ drops out and the strain evaluation

$$\mathbf{E} = \tfrac{1}{2}\big(\mathbf{U}^{\mathrm{T}}\big(\mathbf{R}^{\mathrm{T}}\mathbf{R}\big)\mathbf{U} - \mathbf{1}\big) = \tfrac{1}{2}\big(\mathbf{U}^2 - \mathbf{1}\big) \tag{27}$$

depends solely on the right-stretch tensor $\mathbf{U}$. Thus, a modified right-stretch tensor $\mathbf{U}^{\mathrm{mod}}$ can be computed by employing the polar decomposition to

$$\mathbf{E}^{\mathrm{mod}} = \tfrac{1}{2}\big(\big(\mathbf{U}^{\mathrm{mod}}\big)^2 - \mathbf{1}\big) \Rightarrow \mathbf{U}^{\mathrm{mod}} \tag{28}$$

Finally, the modified deformation gradient

$$\mathbf{F}^{\mathrm{mod}} = \mathbf{R}\mathbf{U}^{\mathrm{mod}} \tag{29}$$

is computed after the multiplication of the unmodified orthogonal rotation tensor $\mathbf{R}$ with the modified right-stretch tensor $\mathbf{U}^{\text{mod}}$.

It must be noted that for the computation of the orthogonal rotation tensor $\mathbf{R}$ a polar decomposition of Equation (25) is necessary. Thus, the method to evaluate the deformation gradient $\mathbf{F}^{\text{mod}}$ which is consistent to the modified strains $\mathbf{E}^{\text{mod}}$ incorporates twice a time-consuming polar decomposition at each integration point.

4.2. Volumetric locking and volumetric locking-free formulations

Plasticity for either small or large deformations is based on incompressible material behaviour. In equivalence to solid elements solid–shell elements without modifications beyond the ones described so far suffer from volumetric locking. This failure is confirmed by the investigation of the eigenvalues and eigenmodes in Section 5.1. Thus, in this section the mostly used approaches to avoid volumetric locking are briefly discussed. A more detailed description is given in the corresponding literature.

Moran and coworkers [16] propose a volumetric locking-free formulation by modifying the deformation gradient (4) in the following form:

$$\tilde{\mathbf{F}} = \left(\frac{\det \mathbf{F}_0}{\det \mathbf{F}} \right)^{1/3} \mathbf{F} \tag{30}$$

In Equation (30), $\mathbf{F}_0$ is the deformation gradient at the element mid-point. Unfortunately, this approach leads to a rather complicated consistent linearization and therefore it cannot be applied easily to the solid-shell formulations described in the previous sections.

Observing the undesired eigenmodes with eigenvalues close to infinity displayed in Figure 5 the idea to assume the normal thickness strain constant in tangent space evolves using the compatible normal thickness strain at the element mid point of each integration point in thickness direction:

$$E_{\zeta\zeta}^{\text{as}}(\xi, \eta, \zeta) = E_{\zeta\zeta}(0, 0, \zeta) \tag{31}$$

In contrast to the previously mentioned approach this assumption can be applied very easily to existing solid-shell element formulations. However, the coupling of the standard in-plane and thickness strains together with the incompressible material behaviour indicated by a Poisson ratio $v \rightarrow 0.5$ are responsible for far too stiff results due to thickness locking (see also Section 2.1.2).

4.2.1. Reduced integration in tangent space.
The misbehaviour mentioned in the last section can be overcome by also assuming the standard in-plane strains to be constant in the tangent space. Thus, if reduced integration in in-plane direction is applied to reduce the computational effort a formulation with additional constant approximation of the in-plane and transverse shear strains in tangent space is obtained. As already mentioned in Section 2.1.1, transverse shear and membrane locking is also avoided by reduced integration:

$$\int_V^{(\text{red})} \left(\delta\mathbf{E} \cdot \frac{\partial\mathbf{S}}{\partial\mathbf{E}} \Delta\mathbf{E} + \Delta\delta\mathbf{E} \cdot \mathbf{S} \right) dV \quad \Delta\mathbf{u} = - \int_V^{(\text{red})} \delta\mathbf{E} \cdot \mathbf{S} \, dV - \delta\Pi_{\text{ext}} \tag{32}$$

However, zero-energy modes occur and therefore complicated stabilization procedures [17] must be applied to achieve reliable element formulations. Solely for the element based on a quadratic Serendipity displacement interpolation in in-plane direction zero-energy modes occur

that cannot appear in most meshes. This formulation is very efficient as far less operations on element level are needed than compared to the solid-shell elements using a bilinear interpolation in tangent space. Responsible for this fact is first the number of integration points which is identical for the quadratic and bilinear elements and second that no additional sampling points for the assumed strain part are necessary. Thus, also no additional time-consuming spectral decompositions (28) and (25) are needed.

4.2.2. Reduced integration of the volumetric term. In this contribution the reduced integration in tangent space of the volumetric term only is proposed to avoid volumetric locking. As usual the developments are based on the weak form

$$\int_V \delta \mathbf{E} \cdot \mathbf{S} \, dV + \delta \Pi_{\text{ext}} = 0 \tag{33}$$

i.e. with the principle of virtual displacements. The strains $\mathbf{E}$ and stresses $\mathbf{S}$ in Equation (33) can be split additively into a volumetric part

$$\mathbf{E}_v = \tfrac{1}{3} \left(E_{\xi\xi} + E_{\eta\eta} + E_{\zeta\zeta} \right) \begin{bmatrix} 1 & 0 & 0 \\ 0 & 1 & 0 \\ 0 & 0 & 1 \end{bmatrix}, \quad \mathbf{S}_v = \tfrac{1}{3} \left(S^{\xi\xi} + S^{\eta\eta} + S^{\zeta\zeta} \right) \begin{bmatrix} 1 & 0 & 0 \\ 0 & 1 & 0 \\ 0 & 0 & 1 \end{bmatrix} \tag{34}$$

and a deviatoric part

$$\mathbf{E}_d = \mathbf{E} - \mathbf{E}_v, \quad \mathbf{S}_d = \mathbf{S} - \mathbf{S}_v \tag{35}$$

By inserting Equations (34) and (35) into Equation (33) the following form is obtained:

$$\int_V \delta \mathbf{E}_d \cdot \mathbf{S}_d \, dV + \int_V \delta \mathbf{E}_v \cdot \mathbf{S}_v \, dV + \int_V \delta \mathbf{E}_d \cdot \mathbf{S}_v \, dV + \int_V \delta \mathbf{E}_v \cdot \mathbf{S}_d \, dV + \delta \Pi_{\text{ext}} = 0 \tag{36}$$

The further developments in this section are based on the assumption that the terms

$$\int_V \delta \mathbf{E}_v \cdot \mathbf{S}_d \, dV = \int_V \delta \mathbf{E}_d \cdot \mathbf{S}_v \, dV = 0 \tag{37}$$

vanish, which is fulfilled by all material laws that can be decoupled into a deviatoric and a volumetric part. Thus, the weak form

$$\int_V \delta \mathbf{E}_d \cdot \mathbf{S}_d \, dV + \int_V^{\text{(red)}} \delta \mathbf{E}_v \cdot \mathbf{S}_v \, dV + \delta \Pi_{\text{ext}} = 0 \tag{38}$$

with reduced integration in in-plane direction of the volumetric part is the basis for all volumetric locking free solid-shell formulations proposed in the following sections.

A simple and efficient algorithm for this non-linear problem is obtained, if the strains are not decoupled, which finally leads to the linearized equation

$$\left\{ \int_V \left(\delta \mathbf{E} \cdot \frac{\partial \mathbf{S}_d}{\partial \mathbf{E}} \Delta \mathbf{E} + \Delta \delta \mathbf{E} \cdot \mathbf{S}_d \right) dV + \int_V^{\text{(red)}} \left(\delta \mathbf{E} \cdot \frac{\partial \mathbf{S}_v}{\partial \mathbf{E}} \Delta \mathbf{E} + \Delta \delta \mathbf{E} \cdot \mathbf{S}_v \right) dV \right\} \Delta \mathbf{u}$$

$$= - \left\{ \int_V \delta \mathbf{E} \cdot \mathbf{S}_d \, dV + \int_V^{\text{(red)}} \delta \mathbf{E} \cdot \mathbf{S}_v \, dV \right\} - \delta \Pi_{\text{ext}} \tag{39}$$

which is necessary for the commonly used Newton–Raphson-type solution method.

It can be concluded that applying the selective reduced integration in tangent space to avoid volumetric locking in addition to the methods described in Sections 2.1.1 and 2.1.2 to prevent from membrane, transverse shear and thickness locking a number of different locking free solid-shell formulations can be derived. As only a separation of the volumetric and the deviatoric parts of the stiffness matrix and the right-hand side vector is necessary the modifications of many well-known formulations can be implemented in a straight forward fashion into a computer program. The only restriction to these formulations is that the material laws must allow a decoupling into a volumetric and deviatoric part. However, for the commonly employed Hencky material law with von Mises plasticity which is also valid for large inelastic deformation problems such a decoupling can be applied easily according to Doll *et al.* [19].

5. NUMERICAL EXAMPLES

The following numerical analyses are performed with quadrilateral, respectively, 8-node hexahedron elements, all incorporating the assumed natural shear (ANS) strain approximation (see Equation (6)). To avoid thickness locking the ANS3Dq solid-shell element employs the quadratic interpolation of the local displacement in thickness direction shown in Equation (12), whereas the ANS3DEAS element is based on the linear enhancement of the normal strains in thickness direction (see Equation (13)). If in addition the in-plane strains of the solid-shell element are enhanced according to Equation (7), then the EAS3DEAS element is obtained. For all these three solid–shell elements a full integration of both, the deviatoric and volumetric term, is used. The corresponding ANS3DqrV, ANS3DEASrV and EAS3DEASrV elements are based on a reduced integration of the volumetric term in tangent space only to remove volumetric locking. Furthermore, the 16-node hexahedron element called S8r3Dq which is especially efficient for materially non-linear problems is investigated. This solid-shell element employs quadratic Serendipity shape functions and a reduced integration in tangent space for all terms together with a quadratic approximation of the displacements in thickness direction following Equation (12) to avoid locking.

5.1. Investigation of eigenvalues and eigenmodes

To get some information about the element behaviour concerning zero-energy modes and possible locking tendencies the eigenvalues of a single element are computed for each element formulation. For this analysis an element shape is chosen that is typical for an element contained in a regular mesh of a square plate (see Figure 4).

Three situations are investigated. First the eigenvalues are computed using Poisson ratios $v = 0.0$ and 0.3 which are displayed Tables I and II. Then the eigenvalues of the square element are investigated for the nearly incompressible range which is indicated by the use of a Poisson ratio of $v = 0.499$ (see Table III). To gain more insight into the behaviour in the limit of incompressibility the eigenmodes of the ANS3DEAS element for the 'infinite' eigenvalues are displayed in Figure 5. It must be noted that the first of these eigenmodes should remain as it is, as no volumetric change is allowed. The other three eigenmodes are responsible for volumetric locking and thus should be avoided.

The EAS3DEAS element with additional enhancement of the in-plane strains still shows one undesired 'infinite' eigenvalue. Obviously, due to the application of the EAS method

$$
\begin{aligned}
l &= 5 \\
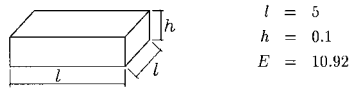h &= 0.1 \\
E &= 10.92
\end{aligned}
$$

Figure 4. Geometry and material data of the square element chosen for the eigenvalue analysis.

Table I. Eigenvalues of a square element: poisson ratio $v = 0.0$.

Element	Rigid-body motion	Kinematics	Eigenvalues			
			<0.1	<1.0	$\approx\infty$	Max
ANS3Dq	1.–6.	—	7.–9.	10.–16.	—	1365
ANS3DEAS	1.–6.	—	7.–9.	10.–16.	—	1365
EAS3DEAS	1.–6.	—	7.–9.	10.–16.	—	1365
ANS3DqrV	1.–6.	—	7.–9.	10.–16.	—	1365
ANS3DEASrV	1.–6.	—	7.–9.	10.–16.	—	1365
EAS3DEASrV	1.–6.	—	7.–11.	12.–16.	—	1365
S8r3Dq	1.–6.	7.–8.	9.–19.	20.–36.	—	2579

Table II. Eigenvalues of a square element: poisson ratio $v = 0.3$.

Element	Rigid-body motion	Kinematics	Eigenvalues			
			<0.1	<1.0	$\approx\infty$	Max
ANS3Dq	1.–6.	—	7.–9.	10.–16.	—	1838
ANS3DEAS	1.–6.	—	7.–9.	10.–16.	—	1838
EAS3DEAS	1.–6.	—	7.–9.	10.–16.	—	1838
ANS3DqrV	1.–6.	—	7.–9.	10.–16.	—	1838
ANS3DEASrV	1.–6.	—	7.–9.	10.–16.	—	1838
EAS3DEASrV	1.–6.	—	7.–11.	12.–16.	—	1838
S8r3Dq	1.–6.	7.–8.	9.–20.	21.–36.	—	3471

for the in-plane strains the third and fourth of the undesired 'infinite' eigenvalues can be avoided.

As already mentioned in Section 4.2.2 with reduced integration of the volumetric term in tangent space the last undesired 'infinite' eigenvalue is removed. Thus, only the desired 'infinite' eigenvalue and the corresponding eigenmode are present.

The additional degrees of freedom necessary for the quadratic displacement interpolation in thickness direction (12) employed for the ANS3Dq and ANS3DqrV elements are responsible for the additional four, respectively, one 'infinite' eigenvalues obtained for these elements. The two 'infinite' eigenvalues and the corresponding eigenmodes of the ANS3DqrV element should be included in a correct formulation, thus this element is free from volumetric locking.

The 16-node element S8r3Dq shows many 'infinite' eigenvalues, as does its fully integrated counterpart. No judgement can be made from a closer look at the eigenmodes and simple conclusions as for the bilinear element cannot be drawn. However, the S8r3Dq element shows

Table III. Eigenvalues of a square element: poisson ratio $v = 0.499$.

Element	Rigid-body motion	Kinematics	Eigenvalues			
			<0.1	<1.0	$\approx \infty$	Max
ANS3Dq	1.–6.	—	7.	8.–15.	21.–28.	$\approx 2 \times 10^5$
ANS3DEAS	1.–6.	—	7.	8.–15.	21.–24.	$\approx 2 \times 10^5$
EAS3DEAS	1.–6.	—	7.	8.–15.	23.–24.	$\approx 2 \times 10^5$
ANS3DqrV	1.–6.	—	7.–9.	10.–15.	27.–28.	$\approx 2 \times 10^5$
ANS3DEASrV	1.–6.	—	7.–9.	10.–15.	24.	$\approx 2 \times 10^5$
EAS3DEASrV	1.–6.	—	7.–11.	12.–15.	24.	$\approx 2 \times 10^5$
S8r3Dq	1.–6.	7.–8.	9.–20.	21.–36.	49.–56.	$\approx 4 \times 10^5$
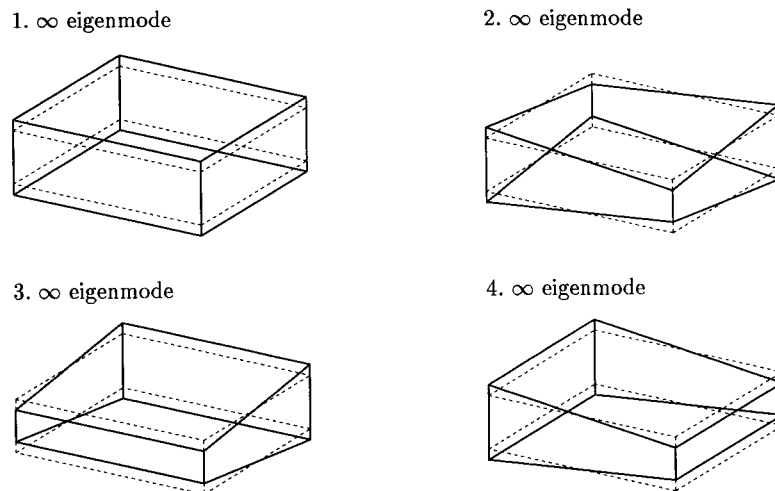
Figure 5. Eigenmodes with 'infinite' eigenvalues in the incompressible limit. ANS3DEAS element.

almost no volumetric locking in the examples analysed. Thus, this is not further investigated here.

In addition, looking at the three undesired eigenmodes with 'infinite' eigenvalues in Figure 5 it can be concluded that a constant approximation of the normal thickness strain in in-plane direction using the value at the element mid point must lead to an element formulation which is free from volumetric locking. This technique is applied leading to the so-called ANS3DEAScT element and the investigation of the eigenvalues confirm this observation. However, due to the coupling of the constant thickness strains with the standard in-plane strains varying linearly in in-plane direction this elements suffers extremely from thickness locking. Therefore, it is not considered any further in the following investigations.
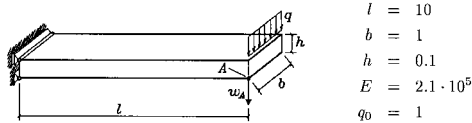
Figure 6. Geometry and material data of the Cantilever beam.

$l = 10$
$b = 1$
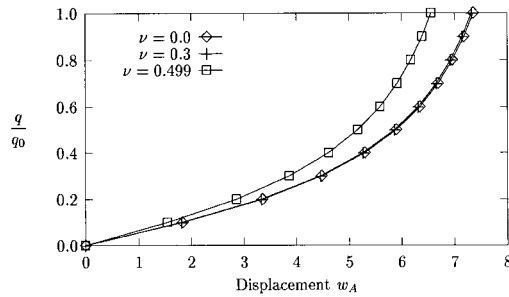$h = 0.1$
$E = 2.1 \cdot 10^5$
$q_0 = 1$

Figure 7. Cantilever beam; $10 \times 1 \times 1$ elements; load deflection diagram; displacement of point A, ANS3Dq element.
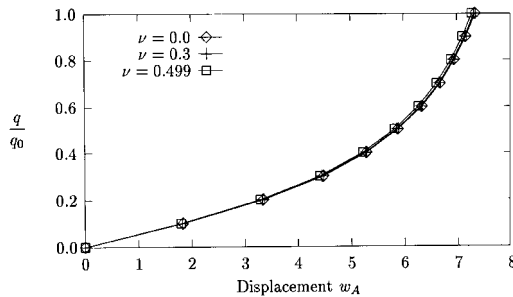

Figure 8. Cantilever beam; $10 \times 1 \times 1$ elements; load deflection diagram; displacement of point A, ANS3DqrV element.

5.2. Varying the Poisson ratio v with linear material models

A cantilever beam subjected to a line load at the end using a discretization with $10 \times 1 \times 1$ elements is investigated. The geometry and the material data for the analyses of the geometrically non-linear problem are given in Figure 6. For brevity reasons only the behaviour of two solid–shell elements is displayed in the following load displacement diagrams in Figures 7 and 8.

From the two curves and further analyses the following is obtained: The behaviour of the EAS3DEAS element is quite similar to the behaviour of the ANS3DEAS element and thus not discussed separately. Comparing the ANS3Dq element with the ANS3DEAS element the influence of the volumetric locking is much smaller for the ANS3DEAS element. This might be due to the fact that the thickness strains are incompatible for the ANS3DEAS element. It is clearly visible in Figure 8 and in further analyses with the S8r3Dq element that the volumetric locking can be reduced drastically by employing selective reduced integration or reduced integration in tangent space. The minor differences between the load displacement curves with various Poisson ratios appear to be due to the influence of the boundary condition keeping the upper and lower points fixed in horizontal direction. Thus, a constraint is introduced which must lead to sightly different results.

$r = 9$
$l = 30$
$h = 2$
$q = 1/30$
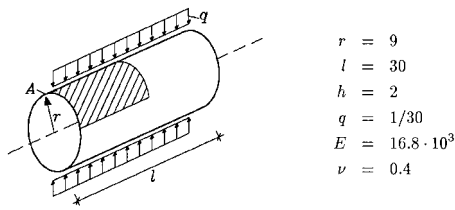$E = 16.8 \cdot 10^3$
$\nu = 0.4$

Figure 9. Geometry, load and material data of the hyper-elastic cylindrical shell.
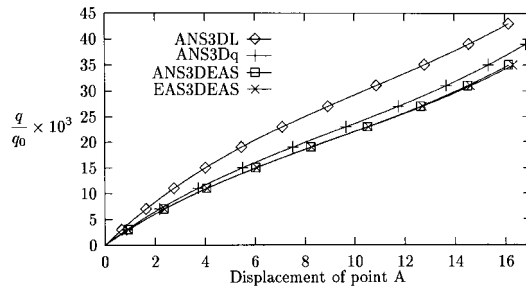

Figure 10. Load versus displacement curves for the hyper-elastic cylindrical shell.
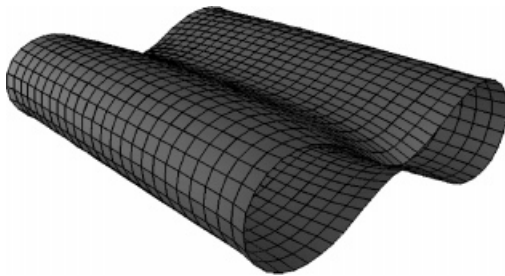

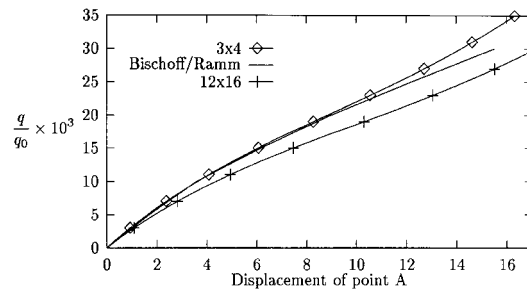Figure 11. Deformed geometry of the hyper-elastic cylindrical shell.

Figure 12. Load versus displacement curves for the hyper-elastic cylindrical shell.

5.3. Large elastic deformations

The analyses described in this section are all performed using the ANS3Dq, ANS3DEAS and EAS3DEAS elements and the Ogden material law with compressible extension as described in Section 3.1. In addition, the eight-node ANS3DL element with assumed shear strains (6) but without any modification to prevent thickness locking is included for comparison reasons.

5.3.1. Hyper-elastic cylindrical shell subjected to a line load. The geometry and material data of the hyper-elastic cylindrical shell subjected to opposite line loads are given in Figure 9. This example is taken from Bischoff and Ramm [33]. The chosen thickness to length ratio h/l accounts for a rather thick shell and thus large deformations occur during the deformation (see Figure 11). Due to the symmetry of the structure only an octant is computed applying symmetry conditions and using a mesh with one element over the thickness, three elements in longitudinal direction and four elements in circumferential direction. For the integration in thickness direction three Gauss points are employed.

In the following diagrams, the load factor versus the vertical displacement of the end of the cylinder is depicted for all elements mentioned above. From the simulations we observe that—as expected—only the ANS3DL element leads to overly stiff results. The minor differences between the load displacement curves of the ANS3Dq and both EAS elements occur due to the

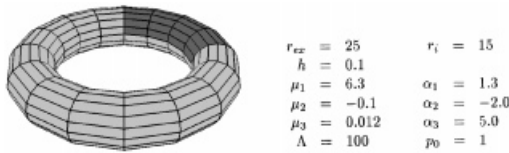*Int. J. Numer. Meth. Engng* 2000; **49**:1121–1141

Figure 13. Geometry and material data of the torus taken from Reference [31].
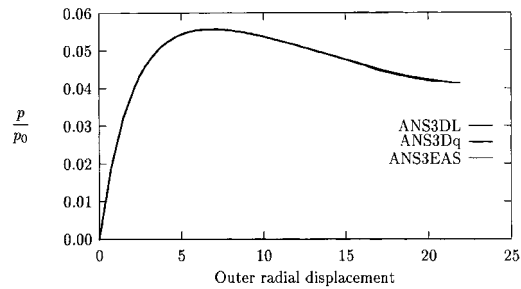

Figure 14. Torus, $4 \times 8 \times 1$ elements; load deflection diagram.

compatible, respectively, incompatible linear enhancement of the originally constant thickness strains. The curves for varying mesh density given in Figure 12 indicate that the original mesh is too coarse to obtain fairly accurate results. Although the results for the coarse mesh compare very well to those obtained by Bischoff and Ramm [33] for smaller displacements, the curves show major differences for increasing deformations. This deviation is due to the material law used by Bischoff and Ramm

$$W = \frac{\lambda}{2}(\ln J)^2 - \mu \ln J + \frac{\mu}{2}(\operatorname{tr} \mathbf{C} - 3) \tag{40}$$

which contains a different compressible extension than the Neo-Hooke material law

$$W = \frac{\lambda}{4}(J^2 - 1 - 2\ln J) - \mu \ln J + \frac{\mu}{2}(\operatorname{tr} \mathbf{C} - 3) \tag{41}$$

which is included in the Ogden material law given in Equation (16) and employed to the solid–shell elements ANS3DL, ANS3Dq, ANS3DEAS and EAS3DEAS in this contribution.

5.3.2. Torus under internal pressure. This example was proposed by Reese [31] to investigate the material stability problem. Again only an octant of the torus with loading p_0, the geometry—radii r_{ex}, r_i, thickness h—and material data for an Ogden material with compressible extension given in Figure 13 is discretized with $4 \times 8 \times 1$ elements applying symmetry conditions. Although solely a symmetric part of the whole structure is investigated, still two of the bifurcation points obtained in Reference [31], where almost the full structure was analysed, were found. Due to the membrane-dominated behaviour of the torus under pressure there are no differences visible in the results between the various solid–shell elements. Convergence problems occur at a displacement of about twenty because then the first bifurcation point is found and path change procedures could be applied. However, such investigations are beyond the scope of this contribution. Some minor differences to the results of Reese [31] are caused by the slightly different discretization chosen.

5.4. Large elastoplastic deformations

For the analyses showing large elastoplastic deformations the fully integrated ANS3Dq, ANS3DEAS and EAS3DEAS and the selective reduced integrated ANS3DqrV, ANS3DEASrV

$$
\begin{aligned}
l &= 508 \\
h &= 2.54 \\
q_0 &= 10^{-2} \\
\kappa &= 57500, \text{bulk modulus} \\
\mu &= 26538, \text{shear modulus} \\
y_0 &= 248, \text{yield stress}
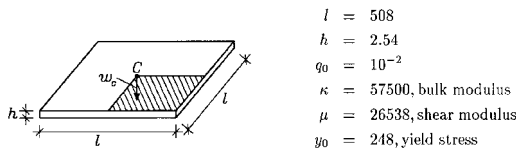\end{aligned}
$$

Figure 15. Geometry and material
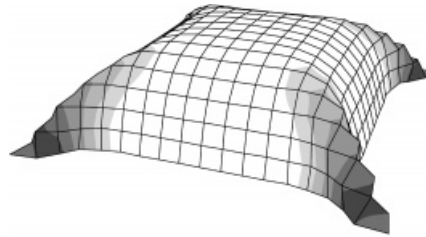data of the square plate.

Figure 16. Deformed geometry and
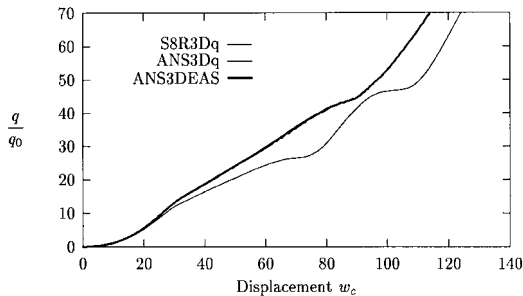plastic zones of the square plate.

Figure 17. Square plate; load deflection diagram; displacement of center point, fully integrated elements and reduced integrated Serendipity element.
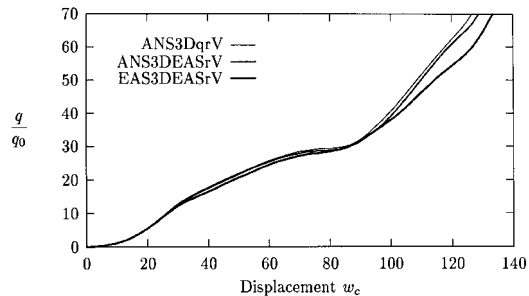

Figure 18. Square plate; load deflection diagram; displacement of center point, elements with selective reduced integration.

and EAS3DEASrV solid–shell elements and the S8R3Dq solid–shell element using the reduced integration in tangent space are investigated. The material behaviour is described by the Hencky material law with von Mises plasticity.

5.4.1. Square plate subjected to uniform loading. First, a square plate which is subjected to uniform loading q_0 with the geometry and material data, ideal elasto-plastic material, given in Figure 15 is analysed. The lower boundary of the plate is fixed in vertical direction whereas the displacements tangential to the plate and the upper boundary are free. After applying the total uniform loading the deformation displayed in Figure 16 is obtained showing also the final plastic zones. Due to symmetry only a quarter is discretized with one element over the thickness and 8×8 elements in tangent plane for the bilinear elements, respectively, 5×5 elements for the biquadratic element. For the integration in thickness direction six Gauss points are used. In Figures 17 and 18, the load displacement curves obtained in 70 load steps are shown.

As expected, the curves coincide for displacements smaller than about 25 whereas the results of the fully integrated elements are clearly very stiff due to incompressibility locking for larger displacements. Although there are solely slight differences visible between the curves obtained by the ANS3DqrV and ANS3DEASrV elements, the additional enhancement of the in-plane strains included in the EAS3DEASrV element is responsible for larger differences.
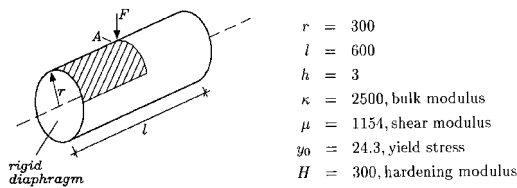
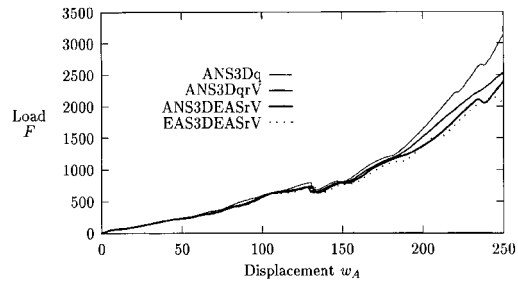Figure 19. Geometry and material data of the pinched cylinder.

$r = 300$

$l = 600$

$h = 3$

$\kappa = 2500$, bulk modulus

$\mu = 1154$, shear modulus

$y_0 = 24.3$, yield stress

$H = 300$, hardening modulus

Figure 20. Pinched cylinder; load deflection diagram; displacement of center point.
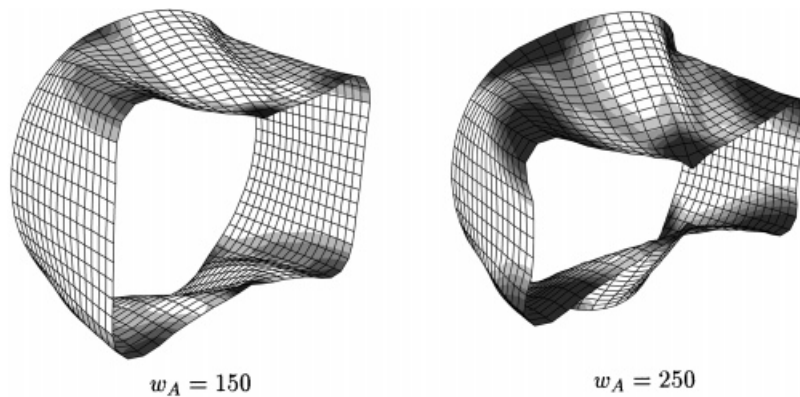

$w_A = 150$ $w_A = 250$

Figure 21. Deformed geometry and plastic zones of the pinched cylinder.

Investigations of Büchter *et al.* [10] achieved by the use of a so-called seven parameter shell element that is based on a biquadratic Serendipity displacement interpolation and reduced integration technique are in full agreement with the load displacement curve of the S8R3Dq element. Although the analyses published in Reference [34] for the same example are based on a finer discretization with $16 \times 16 \times 1$ elements the results are in good equivalence with those obtained by the EAS3DEAS solid-shell element with the coarser discretization used in the current contribution. It must be mentioned that investigations with finer meshes, omitted here for brevity reasons, should be performed to obtain good results thus finally mesh convergence. However, as is well known, the difference in the element behaviour is more pronounced for the chosen coarse mesh.

5.4.2. Pinched cylinder subjected to opposite point loads. Another example employing elasto-plastic material behaviour with kinematic hardening is the pinched cylinder subjected to opposite point loads also previously investigated by Wriggers *et al.* [35] and Miehe [34]. The geometry and material data are given in Figure 19. Due to symmetry, only one-eighth of the cylinder is investigated using—on purpose—a fairly coarse mesh with 16×16 elements in in-plane and one element in thickness direction. The load displacement curves shown in

Figure 20 are obtained by an integration with six Gauss points in thickness direction. Again the results achieved are in full agreement with those published in References [34, 35]. It is clearly visible from the deformed shapes in Figure 21 that the coarse mesh is responsible for the non-physical kinks in the load deflection curves. The coarse mesh resolution chosen for comparison is not capable to capture the sharp curvature in the plastic zone and local snap-through problems are artificially generated which could be completely removed with finer meshes. However, in the latter case the differences in the element behaviour are not visible any more.

6. CONCLUSIONS

In the present contribution an alternative formulation to the established degenerated shell concept developed previously for small strain non-linear analyses is enhanced for large elastic and large elastoplastic deformations and finally applied using some numerical examples.

The necessary enhancements concerning the right Cauchy–Green tensor for hyper-elastic materials, respectively, the deformation gradient for elastoplastic materials, here Hencky material combined with von Mises plasticity, have been presented. It is noted that the modifications are rather elaborate for elastoplastic material.

Several approaches to avoid incompressibility locking are discussed. In the present contribution, the selective reduced integration in tangent space of the volumetric term is favoured and described in detail. Although this technique is limited to the material laws which allow a split into a volumetric and a deviatoric part this limitation has no real disadvantage, commonly used material laws can be easily modified in such a fashion. The application to various numerical examples show that the selective reduced integrated solid-shell elements with reduced integration in tangent space of the volumetric term are very robust and excellent results can be achieved.

REFERENCES

1. Bathe KJ. *Finite Element Procedures in Engineering Analysis*. Prentice-Hall: Englewood Cliffs, NJ, 1982.
2. Ahmad S, Irons BM, Zienkiewicz OC. Analysis of thick and thin shell structures by curved finite elements. *International Journal for Numerical Methods in Engineering* 1970; **2**:419–451.
3. Ramm E. A plate/shell element for large deflections and rotations. In *Formulations and Computational Algorithms in Finite Element Analysis*, Bathe *et al*. KJ (eds). MIT Press: Cambridge, MA, 1977.
4. Mindlin RD. Influence of rotatory inertia and shear in flexural motions of isotropic elastic plates. *Journal of Applied Mechanics* 1951; **18**:31–38.
5. Reissner E. The effect of transverse shear deformation on the bending of elastic plates. *Journal of Applied Mechanics* 1945; **12**:69–76.
6. Hauptmann R, Schweizerhof K. A systematic development of solid-shell element formulations for linear and nonlinear analyses employing only displacement degrees of freedom. *International Journal for Numerical Methods in Engineering* 1998; **42**:49–70.
7. Seifert B. *Zur Theorie und Numerik Finiter elastoplastischer Deformationen von Schalenstrukturen*. Bericht Nr. F96/2, Institut für Baumechanik und Numerische Mechanik, Universität Hannover, 1996.
8. Parisch H. A continuum-based shell theory for non-linear applications. *International Journal for Numerical Methods in Engineering* 1995; **38**:1855–1883.
9. Verhoeven H. *Geometrisch und physikalisch nichtlineare finite Plattenelemente mit Berücksichtigung der Dickenverzerrung. Dissertation*, Reihe Maschinenbau, Technische Universität Berlin, 1992.
10. Büchter N, Ramm E, Roehl D. Three-dimensional extension of non-linear shell formulation based on the enhanced assumed strain concept. *International Journal for Numerical Methods in Engineering* 1994; **37**: 2551–2568.

11. Ogden RW. Large deformation isotropic elasticity—on the correlation of theory and experiment for incompressible rubber-like solids. *Proceedings of the Royal Society of London*, *Series A* 1972; **326**:565–584.

12. Ogden RW. Large deformation isotropic elasticity—on the correlation of theory and experiment for compressible rubber-like solids. *Proceedings of the Royal Society of London*, *Series A* 1972; **328**:567–583.

13. Treolar LRG. The elasticity of a network of long-chain molecules—I and II. *Transactions of the Faraday Society* 1943; **39**:36–41, 241–246.

14. Mooney M. A theory of large elastic deformation. *Journal of Applied Physics* 1940; **11**:3582–3592.

15. von Mises R. Mechanik der festen Körper im plastisch-deformablem Zustand. Nachrichten von der Gesellschaft der Wissenschaften zu Göttingen. Mathematisch-Pysikalische Klasse 1913; 582–592.

16. Moran B, Ortiz M, Shih CF. Formulation of implicit finite element methods for multiplicative finite deformation plasticity. *International Journal for Numerical Methods in Engineering* 1990; **29**:483–514.

17. Gebhardt H. Finite Element Konzepte für schubelastische Schalen mit endlichen Drehungen. *Dissertation*, Institut für Baustatik, Universität Karlsruhe, 1990.

18. Liu CH, Hofstetter G, Mang HA. 3D Finite element analysis of rubber-like materials at finite strains. *Engineering Computers* 1994; **11**:111–128.

19. Doll S, Hauptmann R, Freischläger C, Schweizerhof K. On volumetric locking of low-order solid and solid–shell elements for finite elastoviscoplastic deformations and selective reduced integration. *Engineering Computations* 2000; to appear.

20. Hakula H, Leino Y, Pitkäranta J. Scale resolution, locking, and high-order finite element modeling of shells. *Journal of Computational and Applied Mathematics* 1996; **133**:157–182.

21. Bucalem EN, Bathe KJ. Higher-order MITC general shell elements. *International Journal for Numerical Methods in Engineering* 1993; **36**:3729–3754.

22. Rhiu JL, Lee SW. A new efficient mixed formulation for thin shell finite element models. *International Journal for Numerical Methods in Engineering* 1987; **24**:581–604.

23. Huang HC, Hinton E. A new nine node degenerated shell element with enhanced membrane and shear interpolation. *International Journal for Numerical Methods in Engineering* 1986; **22**:73–92.

24. Bathe KJ, Dvorkin E. A continuum mechanics based four-node shell element for general nonlinear analysis. *Engineering Computation* 1984; **1**:77–88.

25. Simo JC, Rifai MS. A class of mixed assumed strain methods and the method of incompatible modes. *International Journal for Numerical Methods in Engineering* 1990; **29**:1595–1638.

26. Wilson EL, Taylor RL, Doherty WP, Ghaboussi J. Incompatible displacement models. In *Numerical and Computational Methods in Structural Mechanics*, Fenves ST *et al.* (eds). Academic Press: New York, 1973; 43–57.

27. Braun M. *Nichtlineare Analysen von geschichteten elastischen Flächentragwerken*. Bericht Nr. 19. Institut für Baustatik, Universität Stuttgart, 1995.

28. Hauptmann R. Strukturangepaßte geometrisch nichlineare Finite Elemente für Flächentragwerke. *Dissertation*. Institut für Mechanik, Universität Karlsruhe, 1997.

29. Sansour C. A theory and finite element formulation of shells at finite deformations involving thickness change. *Archive of Applied Mechanics* 1995; **65**:194–216.

30. Gruttmann F. *Theorie und Numerik dünnwandiger Faserverbundstrukturen*. Bericht Nr. F96/1, Institut für Baumechanik und Numerische Mechanik, Universität Hannover, 1996.

31. Reese S. Theorie und Numerik des Stabilitätsverhaltens hyperelastischer Festkörper. *Dissertation*, Technische Hochschule Darmstadt, 1994.

32. Hencky H. The elastic behaviour of vulcanized rubber. *Journal of Applied Mechanics* 1933; **1**:45–53.

33. Bischoff M, Ramm E. *Three-dimensional shell formulation and elements for large deformations*. IUTAM: Wien 1997.

34. Miehe C. A theoretical and computational model for isotropic elastoplastic stress analysis in shells at large strains. *Computer Methods in Applied Mechanics and Engineering* 1998; **155**:193–234.

35. Wriggers P, Eberlein R, Reese S. A comparison of 3-dimensional continuum and shell elements for finite plasticity. *International Journal of Solids and Structures* 1996; **33**:3309–3326.

36. Betsch P, Stein E. An assumed strain approach avoiding artificial thickness straining for a non-linear 4-node shell element. *Communications in Numerical Methods in Engineering* 1995; **11**:899–909.